RSC Advances

PAPER

View Article Online
View Journal | View Issue

Cite this: *RSC Adv.*, 2016, **6**, 1611

A facile way to prepare nanoporous PbI_2 films and their application in fast conversion to $CH_3NH_3PbI_3$†

Huifeng Zheng,[a] Weiqi Wang,[a] Songwang Yang,[b] Yangqiao Liu*[a] and Jing Sun*[a]

Received 13th October 2015
Accepted 17th December 2015

DOI: 10.1039/c5ra21250b

www.rsc.org/advances

In this report, we demonstrate a facile way to prepare PbI_2 films with interpenetrating nanopores. The nanoporous PbI_2 (n-PbI_2) films were prepared by the solvent–solvent extraction (SSE) method, in which the DMF solvent was effectively extracted by isopropanol (IPA) within seconds, resulting in well-crystallized n-PbI_2 films without annealing. The mechanism involved in the preparation of n-PbI_2 films using the SSE method was studied further, and some universal rules for fabricating n-PbI_2 films with the SSE method were proposed. The interpenetrating nanoporous morphology enabled fast penetration of the CH_3NH_3I (MAI) solution, so most of the PbI_2 converted into $CH_3NH_3PbI_3$ within 10 s even with a perovskite overlayer of 300 nm. Moreover, the perovskite layer was pinhole-free and smoother than that based on a conventional PbI_2 film. Consequently, perovskite solar cells based on n-PbI_2, with the setup as FTO/compact TiO_2/bilayer $CH_3NH_3PbI_3$/P3HT/Ag, delivered an impressive power conversion efficiency of 10.1%, compared with 5.9% for its counterpart based on a conventional compact PbI_2 film. This work unveils the PbI_2-morphology-related reaction kinetics in the two-step method, and will contribute to understanding the role PbI_2 films play in the preparation of perovskites.

Introduction

Organometal halide perovskites have been a hot topic in the field of solar cells, due to their excellent properties such as a high extinction coefficient,[1] long carrier diffusion length[2–4] and a tunable bandgap.[5–9] Recently, their power conversion efficiencies has reached over 20%.[10] Perovskite films are usually prepared by three methods: (1) one-step solution deposition;[11,12] (2) two-step solution deposition;[13] (3) vapor deposition.[14,15] Generally, the two-step method offers better control of the films' morphology than the one-step method,[16,17] and is much cheaper, and more convenient than the vapor deposition.

The critical step in the two-step method is dipping PbI_2 films into CH_3NH_3I (MAI) solution to react. However, the reaction takes tens of minutes to 2 hours, for planar structure[13,18] or bilayer structure[19,20] comprising mesoscopic and planar layers.[21–23] However, dipping too long results in: (1) the abnormal growth of perovskite crystals;[23,24] (2) the dissolution or peel-off of perovskite films,[18,25] both of which will deteriorate the efficiency. To shorten the dipping time, isopropanol (IPA) pre-wetting[13,26] and increasing reaction temperature[26–28] are common practices. However, both of them accelerates the reaction between PbI_2 and CH_3NH_3I as well as the abnormal growth of perovskite crystals,[26] detrimental to the reproducibility.[27] So, it is in great demand for a facile method to accelerate the reaction without causing the abnormal growth of perovskite crystals for planar and bilayer structure.

Recently, some researchers proposed the application of porous PbI_2 films to facilitate the reaction.[29,30] As the reaction between PbI_2 (solid) and MAI (in IPA) is essentially a solid–liquid reaction, the larger specific area is the more reaction sites there are, promising a higher reaction rate.[25]

However, in those reports the porous PbI_2 films consisting of nano-sheet arrays were fabricated by vacuum thermal evaporation, which was too complex for preparation and not energy-saving.[29,30] Furthermore, porous PbI_2 was attainable only when polycrystalline substrates were applied.[29] Besides, Zhou *et al.* prepared nanoporous PbI_2 (n-PbI_2) by air blowing and drying at room temperature.[31] Whereas, this method takes several hours to prepare, due to the low volatility of the solvent (dimethyl formamide, DMF) at room temperature. Here, we demonstrate a facile way to synthesize PbI_2 films with interpenetrating nanopores by the solvent–solvent extraction (SSE) method.[32] The SSE is a process in which solute crystallized as a result of extracting the main solvent by another poor solvent. The SSE process was first reported in the fabrication of perovskite layers with the one-step method, but never reported in preparing nanoporous PbI_2 films. Using this method, it only takes less than 1 min to prepare well-crystallized nanoporous PbI_2 films without annealing. As expected, the resultant n-PbI_2 films

[a]*State Key Laboratory of High Performance Ceramics and Superfine Microstructure, Shanghai Institute of Ceramics, Chinese Academy of Sciences, 1295 Dingxi Road, Shanghai 200050, P. R. China. E-mail: yqliu@mail.sic.ac.cn; jingsun@mail.sic.ac.cn*

[b]*CAS Key Laboratory of Materials for Energy Conversion, Shanghai Institute of Ceramics, Chinese Academy of Sciences, 588 Heshuo Road, Shanghai 201899, P. R. China*

† Electronic supplementary information (ESI) available. See DOI: 10.1039/c5ra21250b

significantly accelerate the reaction rate. Most part of PbI_2 in n-PbI_2 films converted into perovskite within 10 s, in stark contrast to the 10 min which was needed for conventional compact PbI_2 films. By dipping for 40 s, we obtained pinhole-free bilayer-structured perovskite films with 300 nm overlayer, resulting in the champion efficiency above 10%.

Experimental

Materials

In the fabrication of perovskite and hole transporting layers, all solvents involved were dehydrated by molecular sieves (4A), such as dimethyl formamide (DMF), isopropanol (IPA), toluene. All other materials were used as received.

CH_3NH_3I was prepared according to literature.[15] Specifically, 50 mL methylamine (33 wt%, in absolute ethanol, Aldrich) and 20 mL hydriodic acid (57 wt% in water, J&K Scientific) were reacted in a 500 mL round-bottom flask in the ice bath with stirring under N_2 for 2 h. After that, the solution was evaporated at 50 °C for 1 h to obtain yellowish precipitate, which was washed with diethyl ether twice. Finally, the solid was dried at 60 °C in vacuum for 24 h.

Fabrication of perovskite solar cells

Fluorine-doped tin oxide (FTO; 15 Ω $\square^{-1}$, Nippon Sheet Glass) glass substrates were patterned by Zn powder and HCl (concentrated $HCl : H_2O = 2 : 3$ by volume) for 90 s. The resultant FTO substrates were cleaned sequentially in detergent (Hellmanex II, 2%), water, ethanol, acetone, ethanol with ultrasonication for 30 min and then treated with ultraviolet (UV) for 15 min. A 30 nm thick TiO_2 compact layer was then deposited by spin coating at 6000 rpm for 30 s with a weakly acidic solution of titanium isopropoxide (Aldrich) reported by Snaith's group.[33] After drying at 70 °C, the films were annealed at 500 °C for 30 min. Then, the films were treated in 40 mM $TiCl_4$ aqueous solution for 30 min at 70 °C, rinsed with deionized water and ethanol and dried at 500 °C for 30 min.

The mesoporous TiO_2 was prepared with reported method.[13] After drying at 70 °C, the TiO_2 films were sintered at 500 °C for 30 min. Then, the resultant films were treated with 40 mM $TiCl_4$ for another 30 min, followed by being annealed at 500 °C for 30 min. The mesoporous TiO_2 films were filled by spin coating of 1 M PbI_2 (Sigma) in DMF at 4000 rpm with (for preparing n-PbI_2 films) or without (for preparing c-PbI_2 films) SSE post-treatment. The SSE process was that 100 μL IPA solution was dispensed on the surface of pristine PbI_2 films (without annealing) for several seconds, then spin at 4000 rpm for 60 s. The resultant PbI_2 films were dried at 75 °C for 30 min, before cooling down to room temperature. For preparation of perovskite films, the PbI_2 films were dipped into 10 mg mL^{-1} MAI in IPA for tens of seconds, which was kept at 50 °C. After being rinsed with IPA, the perovskite films were dried at 75 °C for 30 min. When those substrates cold down, a solution of poly-3-hexylthiophene (P3HT: J&K Scientific, RMI-001EE) was spin-coated, whose composition was: P3HT/toluene 15 mg mL^{-1}, 7.5 μL Li-bis(trifluoromethanesulfonyl)imide (Li-TFSI, Aldrich)/acetonitrile (170 mg/1 mL) and 7.5 μL 4-*tert*-butylpridine (*t*-BP, Aldrich)/acetonitrile (1 mL/1 mL).[34] All these steps involving perovskite films and P3HT layer were conducted inside an Ar-filled glovebox. Finally, ~80 nm Ag was thermally evaporated through a shadow mask under vacuum (*ca.* 3×10^{-3} Pa). The effective area for device was 0.15 cm^2.

Characterization

X-ray diffraction (XRD) spectra were obtained from Rigaku D/max 2550V with Cu Kα radiation at a step size of 0.02°. The absorption spectra of perovskite films were characterized by a UV/Vis/NIR spectrophotometer (Lambda 950, Perkin Elmer). The composition of chemical bonding was measured by Fourier Transform Infrared Spectroscopy (FTIR) with Bruker, Tensor 27 using the standard Pike ATR cell. The morphology of perovskite films was observed by scanning electron microscopy (SEM; SU8220, Hitachi, Japan). PbI_2 nanoparticles, scratched from PbI_2 films, were characterized by transmission electron microscopy (TEM; 2100F, JEOL, Tokyo, Japan). The photocurrent–voltage characteristics of perovskite solar cells were measured with Keithley 2400 source meter under the simulated AM 1.5G illumination (100 mW cm^{-2}; Oriel Sol3A Class AAA Solar Simulator, Newport) calibrated with optical power meter (Newport, 1918-R). The *I–V* curves were obtained through reverse scan (1 V to −0.1 V) with step size of 11 mV and delay time of 20 ms. IPCE spectra were measured by a Newport QE system equipped with a 300 mW xenon light and a lock-in amplifier. All samples for characterization were prepared on the substrates FTO/compact TiO_2/mesoporous TiO_2 with the same procedure of preparing thin films applied in solar cells, unless stated otherwise.

Result and discussion

Buildup of nanoporous PbI_2 films and its mechanism

Fig. 1a presents the procedure for preparation of nanoporous PbI_2 film, whose critical step is dropping IPA onto the surface of the as-prepared PbI_2 film. Within seconds after dropping of IPA, the as-spin-coated PbI_2 film turned to dark yellow from pale yellow, indicating the fast formation of PbI_2. Compared with compact c-PbI_2 film (Fig. 1b) prepared by the conventional method, the resultant PbI_2 film was nanoporous, with pores evenly distributed on the surface of the film, as shown by Fig. 1c. The pore size ranged widely, from 30 nm to 200 nm. To research the distribution of pores inside the n-PbI_2 films, we characterized the cross-section of a planar n-PbI_2 film with ~450 nm in thickness (Fig. 1d and e). Fig. 1d and e show that the n-PbI_2 film is nanoporous throughout the entire thickness, different from c-PbI_2 films reported previously which are totally compact.[35,36] Furthermore, it demonstrates the effectiveness of the SSE method to prepare n-PbI_2 films with thickness up to sub-micrometer.

To gain insight into the preparation mechanism of n-PbI_2 films, XRD spectra were collected in the progression of the SSE process, shown in Fig. 2. Film A was spin-coated from PbI_2 solution (in DMF), whose colour is pale yellow. Wakamiya *et al.*

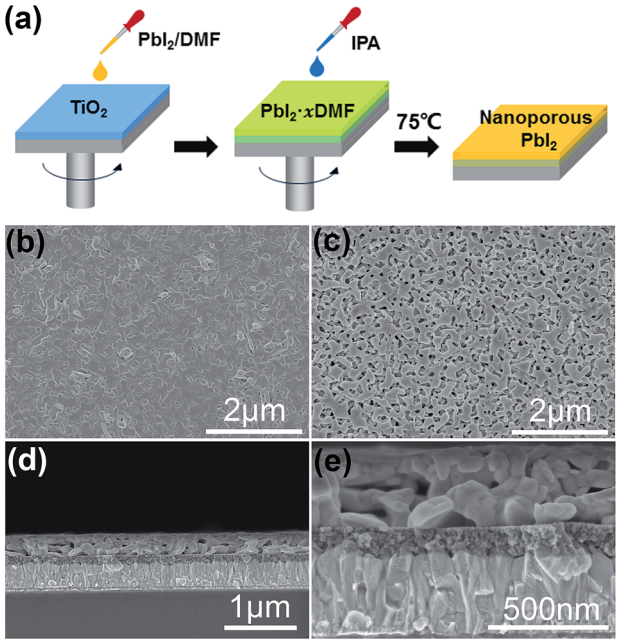

Fig. 1 (a) Procedure for preparing nanoporous PbI_2 film. PbI_2 solution is spin-coated onto the mesoporous TiO_2 film. Then, the resultant film is dropped with IPA for several seconds before spinning off the remained solvent. Finally, the film is heated at 75 °C. SEM images of (b) c-PbI_2 film prepared with the conventional method and (c) n-PbI_2 film prepared with the SSE method. Cross-sectional SEM images of planar n-PbI_2 film with (d) low magnification and (e) high magnification. The planar n-PbI_2 film was prepared by spin coating 1 M PbI_2 (in DMF) at 2000 rpm, followed by SSE process with IPA for 10 s.

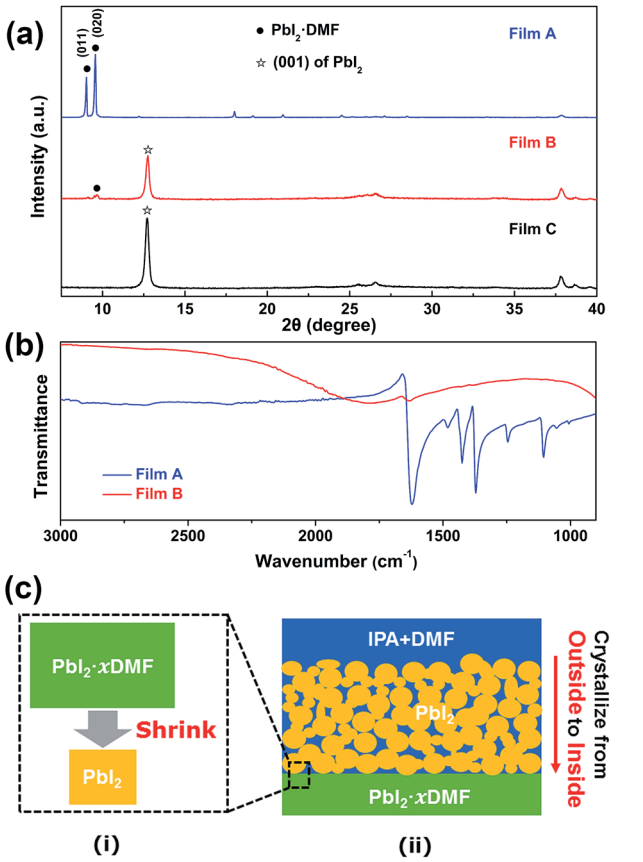

Fig. 2 (a) XRD and (b) FTIR spectra of as-spin-coated PbI_2 film without any treatment (Film A), after SSE process for 10 s without annealing (Film B) and with annealing (Film C). The characteristic peaks of $PbI_2 \cdot DMF$ at 9.02° and 9.56° are corresponding to (011) and (020) planes, respectively. (c) Schematic illustration of the SSE process in preparation of nanoporous PbI_2 films. (i) The volume shrink phenomenon in the transformation from $PbI_2 \cdot xDMF$ to PbI_2. (ii) Crystal growth model of n-PbI_2 film. Until spin off the excessive solvent, IPA was penetrating into the nanoporous PbI_2 frame which had already formed, so PbI_2 crystallized gradually from outside to inside.

demonstrated that the pale yellow crystal was $PbI_2 \cdot DMF$, with one DMF molecule coordinated to Pb forming one-dimensional structure along its *a*-axis.[37] It shows two strong peaks at 9.02° and 9.56° corresponding to (011) and (020) planes of $PbI_2 \cdot DMF$, respectively. That is consistent with other reports, except that the relative intensity of the former peak is higher in our study, as shown in Fig. S1a.†[37,38] After the SSE process (without annealing), the resultant dark yellow film (Film B) showed a strong peak at 12.68° corresponding to (001) lattice plane of PbI_2 (Fig. 2a-red curve), which testifies the crystallization of PbI_2. Meanwhile, the peaks of $PbI_2 \cdot DMF$ decreased to be negligible, indicating the effective extraction of DMF molecular from $PbI_2 \cdot DMF$ by IPA. The extraction of DMF by IPA was confirmed by FTIR characterization as well. As shown in Fig. 2b, the C=O stretching band at ~1650 of DMF (shown in Fig. S1c†) disappeared, indicating most of DMF is removed. Upon further annealing, the (001) peak of PbI_2 became sharper, while the peaks corresponding to $PbI_2 \cdot DMF$ disappeared completely, resulting in a highly crystallized nanoporous PbI_2 film. Furthermore, the nanoporous PbI_2 film showed similar XRD pattern with that from conventional method, indicating that the SSE process would not change the preferential orientation or crystallinity of PbI_2 film deposited on a mesoporous TiO_2 layer, as shown in Fig. S1b.†

Based on the analyses of XRD and FTIR spectra in the evolution of SSE process, we propose a mechanism schematically, as shown in Fig. 2c. The main reaction in SSE process is listed as follows:

$$PbI_2 \cdot xDMF \xrightarrow{IPA} PbI_2(s) + xDMF(l)$$

here we cautiously use $x(x \geq 1)$ rather than precise stoichiometric ratio, because it is possible that some DMF molecules remain in the film without coordinating to PbI_2, as the case of PbI_2–DMSO films.[18] As the reaction equation shows, PbI_2 precipitates immediately once IPA contacts with $PbI_2 \cdot DMF$ film, because the extraction of DMF by IPA will dramatically increase the supersaturation of PbI_2. Moreover, the density of PbI_2 crystal (6.1 g cm^{-3}) is much larger than that of $PbI_2 \cdot DMF$ (3.7 g cm^{-3}),[37] not to speak of the $PbI_2 \cdot xDMF$ films. So, the fast transformation from $PbI_2 \cdot xDMF$ to PbI_2 will lead to a shrink in volume (Fig. 2c), resulting in many nanopores. As Fig. 2c shows, the nanopores formed outside, resulting from the volume shrinkage, facilitates further penetration of the IPA liquids deeper inside the film. Therefore, this solvent extraction reaction can take place thoroughly. As a result, well-structured

interpenetrating pores are developed in the entire thickness. This structure is important for the subsequent perovskite conversion reaction. Note that the structure-building process tactfully utilizes the volume shrink effect in the direction from outside to inside rather than the reverse direction as the conventional annealing method does. In conclusion, the PbI_2 film crystallizes from outside to inside with volume shrink as time goes on before spinning off the solvent, resulting in the interpenetrating nanoporous microstructure throughout the entire thickness.

While the DMF (precursor solvent)/IPA (extraction solvent) combination reported here is just a typical example for preparation of n-PbI_2 films with the SSE method, wide choices of precursor/extraction solvent combination are suitable for it. For example, DMF/toluene combination can be used to prepare n-PbI_2 films, as Fig. S2† shows. Here, we propose some general rules for preparing n-PbI_2 films using the SSE process: (1) the precursor solvents should have high solubility for PbI_2. And a high boiling point is preferred, preventing the evaporation-induced crystallization of PbI_2; (2) the extraction solvent should have low solubility for PbI_2 and relatively low boiling point, in order to dry the films quickly; (3) high intermiscibility between precursor and extraction solvents is necessary, enabling fast SSE process for preparation of n-PbI_2 films.[32]

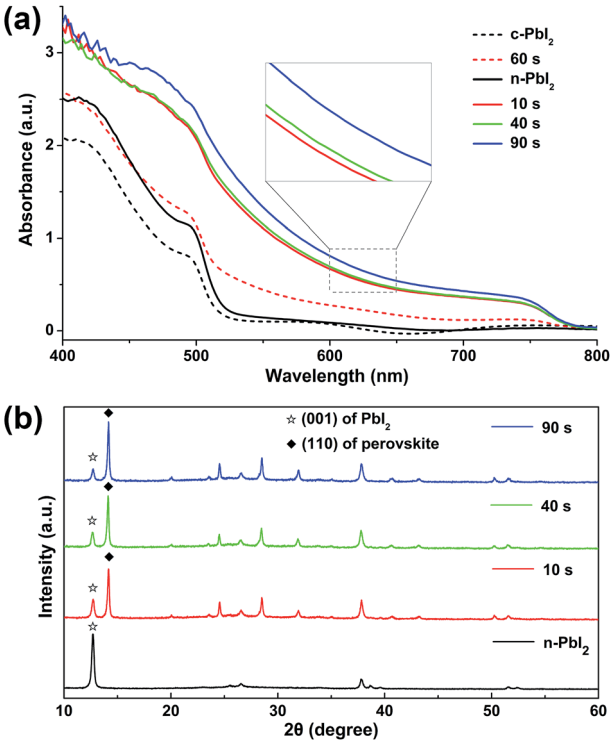

Fig. 3 Effect of dipping time in MAI solution (10 mg mL^{-1}, in IPA) on the evolution of (a) UV-vis absorption spectra and (b) XRD spectra of perovskite films based on c-PbI_2 films (short dash lines) and n-PbI_2 films (solid lines).

Comparison of c-PbI_2 and n-PbI_2 films for conversion to perovskite

To demonstrate the advantages of nanoporous PbI_2 films in preparing perovskite films, we carried out absorption test and XRD characterization in the evolution of PbI_2 conversion into perovskite. As Fig. 3a shows, n-PbI_2 film has a higher absorbance than c-PbI_2, which may come from the light trapping effect of nanoporous morphology. As a result, the photograph (Fig. S3a†) shows n-PbI_2 film is less transparent than c-PbI_2 film. For n-PbI_2 film, the absorbance increases dramatically in the first 10 s when dipped in MAI solution, indicating the fast formation of perovskite. That is confirmed by the XRD test, as shown by Fig. 3b, where the (001) peak of PbI_2 (near 12.6°) is weak compared with the (110) peak of perovskite (near 14.1°).[39] As the reaction goes on, the absorbance of the film increases a little (Fig. 3a) and the peaks of PbI_2 in XRD spectra recede (Fig. 3b). Though trace of PbI_2 remained after reacting for 90 s, some reports showed that the remnant PbI_2 would not deteriorate the performance of solar cells.[23,40] While the c-PbI_2 film shows a different conversion behaviour, as shown in Fig. S4.† When c-PbI_2 film is dipped into MAI solution for 1 min, the absorbance changes little compared with that of c-PbI_2, suggesting that the reaction is slow. The slowness of the reaction is also confirmed by XRD characterization. As Fig. S4b† shows, the (110) peak of perovskite is extremely weak when dipped for 1 min. Although the intensity of perovskite peak increases with the receding of PbI_2 peak as dipping time prolongs, there is still a noticeable amount of PbI_2 remained as indicated by the characteristic PbI_2 diffraction peak. The PbI_2 peak disappears until dipping for as long as 30 min. However, dipping too long results in the dissolution of perovskite film, shown by a weaker absorbance as dipping time increases from 10 min to 30 min (Fig. S4a†), reported by Zhao and Zhu as well.[25] Furthermore, prolonging the dipping time will result in the abnormal growth of perovskite crystals, as shown by Fig. S5,† enhancing surface recombination as a result of the direct contact between Ag and perovskite layers.[41]

Taking into consideration that the reaction between PbI_2 and MAI is a solid–liquid reaction, we believe that the reaction rate is determined by three factors: (1) temperature of the reaction system; (2) concentration of MAI solution (keep the solvent as IPA); (3) properties of PbI_2 films, such as preferential orientation of crystals, crystallinity and morphology of PbI_2 films. In our study, the first two factors have been carefully controlled. And both of preferential orientation and crystallinity in c-PbI_2 film and n-PbI_2 film shows no difference, as shown in Fig. S1b.† So we believe that the great difference between c-PbI_2 and n-PbI_2 films in the preparation of perovskite comes from the morphology difference, as shown in Fig. 4. Mainly, two factors contribute to the faster conversion of n-PbI_2 into perovskite than c-PbI_2: firstly, the interpenetrating nanoporous morphology enables the reaction happened in the entire film simultaneously with much more reaction sites, while the reaction is mainly limited to flat surface in the case of c-PbI_2 films; secondly, both of the particle size and crystallite size are lower in the n-PbI_2 than those of c-PbI_2, as shown in Fig. 1b and c and S6,† shortening the diffusion length for MAI.[43] In a word, the reaction is limited by the interface of PbI_2(s)–MAI(l), so the morphology of PbI_2 films does matter in the two-step method.

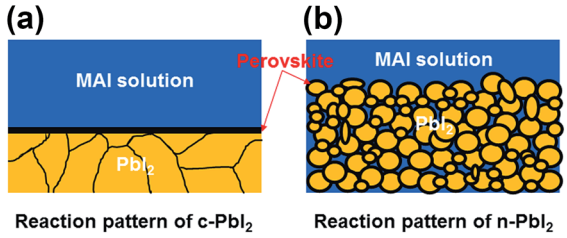

Fig. 4 Reaction patterns of (a) c-PbI_2 film and (b) n-PbI_2 film in the conversion of PbI_2 into $MAPbI_3$ perovskite. The c-PbI_2 film consists of large pancake-like layer crystals (200–300 nm), which is so compact that only little MAI solution is able to penetrate into inside through the crystal interfaces.[42] As a result, the reaction is confined to the surface and some interfaces of crystals. Consequently, the reaction is controlled by the diffusion of MAI in the formed perovskite layers.[43] While the n-PbI_2 film is composed of smaller crystals (50–150 nm) with nanoporous morphology, so that MAI is able to penetrate into nanoporous PbI_2 frame once dipped into MAI solution. Therefore, the reaction is going on within the entire film with large surfaces simultaneously. Moreover, the crystals in n-PbI_2 film are much smaller than those in c-PbI_2 film, accelerating the reaction further.

Though Ko *et al.* tried to show the importance of PbI_2 morphology in the two-step method, they failed to exclude the influence of crystallinity difference of PbI_2.[44] In this study, however, we succeed to demonstrate the important role of the PbI_2 morphology in the conversion of PbI_2 into perovskite without the interference of crystallinity difference, as shown in Fig. S1b.†

There may be a question about the compactness of the perovskite overlayer in the bilayer-structured solar cells, as n-PbI_2 films are nanoporous. To our surprises, the n-PbI_2 based perovskite overlayer is really compact without any obvious pinholes, as shown in Fig. 5a and b and S7,† which can be explained by the volume expansion from the originally edge-sharing octahedral PbI_2 framework (density 6.16 g cm^{-3}) to the corner-sharing octahedral structure in perovskite (density 4.16 g cm^{-3}).[15,45] Specifically, for 1 mol PbI_2 precursor, its volume evolved from 74.8 cm^3 to 149.0 cm^3 in the conversion of PbI_2 into $CH_3NH_3PbI_3$, consistent with previous report.[45] The compactness of the perovskite overlayer is testified by the cross-sectional SEM image of a typical perovskite solar cell as well, shown in Fig. 5e. As Fig. 5e shows, a compact perovskite overlayer of 300 nm covers on a 200 nm mesoporous layer, without any pinholes. Contrastively, some micro-size crystals grow on surface of c-PbI_2 based perovskite film when c-PbI_2 was dipped into MAI solution for 10 min in order to complete the conversion, as shown in Fig. 5c and d. In conclusion, our method manages to fabricate relatively smooth perovskite films without pinholes on the premise that PbI_2 is able to convert into perovskite completely and quickly.

Photovoltaic performance of perovskite solar cells

Fig. 6a shows *J–V* curves of the champion devices with bilayer structure based on n-PbI_2 and c-PbI_2 films, respectively. The solar cell based on n-PbI_2 shows much better performance than that of c-PbI_2, with V_{oc} and J_{sc} improved for 0.1 V and 1 mA cm^{-2}, respectively. While the biggest difference lies in the fill factor (FF), which increases from 0.43 to over 0.6 when n-PbI_2 film replaces c-PbI_2 film resulting in a much shorter reaction time in MAI solution.

The improvement of V_{oc} and FF mainly came from the suppression of surface recombination, by avoiding the direct contact between Ag and perovskite layers in our case.[41] For n-PbI_2, 40 s was enough for the conversion, which was too short for the abnormal growth of perovskite crystals, indicated by Fig. 5a and b. As a result, the perovskite can be covered evenly by a thin P3HT layer avoiding the direct contact between Ag and perovskite, indicated by the smooth Ag layer shown in Fig. 5e. On the contrary, c-PbI_2 based perovskite layer became too rough to be completely covered by P3HT layer, when dipped too long for the sake of complete conversion into perovskite (as shown in Fig. S5†). Another factor deteriorating the FF in c-PbI_2 based solar cells may come from the reactive Ag electrode. The contact between Ag and $CH_3NH_3PbI_3$ results in the insulated AgI layer,[46] whose E_{VB} (−6.88 eV (ref. 47)) is more negative than that of

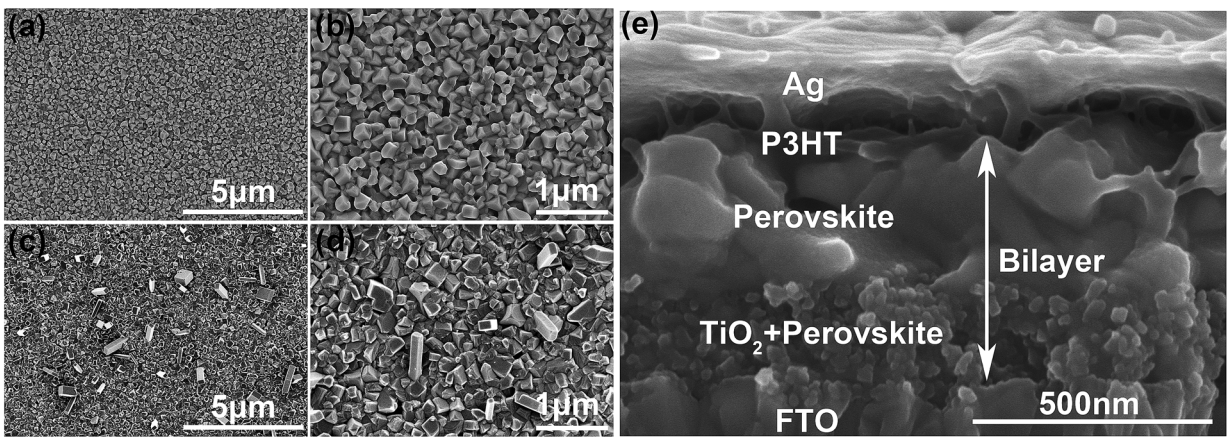

Fig. 5 SEM images of perovskite based on n-PbI_2 film (a) and (b) and based on c-PbI_2 film (c) and (d). Perovskite films were prepared by dipping n-PbI_2 and c-PbI_2 films into MAI solution (10 mg mL^{-1}, in IPA) for 40 s and 10 min, respectively. (e) Cross-sectional SEM image of perovskite solar cell with bilayer structure. The perovskite overlayer is compact without any obvious pinholes, whose thickness is ~300 nm.

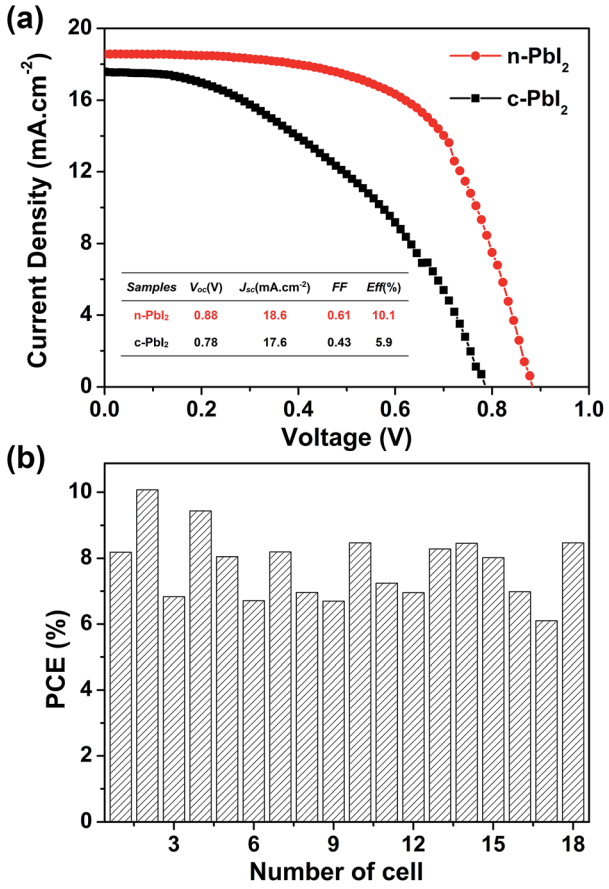

Fig. 6 (a) The best photovoltaic performance of devices based on n-PbI_2 and c-PbI_2 films, which are dipped in MAI solution for 40 s and 10 min, respectively. Both of the dipping time were determined to be optimal in the preliminary tests. (b) Histogram of power conversion efficiency of perovskite films based on n-PbI_2 films.

$CH_3NH_3PbI_3$ (−5.43 eV (ref. 11)), making it impossible for holes to inject into AgI. As a result, it may cause more severe recombination between electrons and holes in $CH_3NH_3PbI_3$ layer. While that will not happen in the case of Au electrode. Therefore, FF of c-PbI_2 based solar cell, even with a thin layer of P3HT, is much lower than that of HTM-free case with Au as back electrode.[41] Those reasons mentioned above contribute to the slight rise in J_{sc} of n-PbI_2 based solar cell as well, apart from the enhanced absorption of perovskite layer resulting from the reflection of smooth Ag layer.[41] As a consequence, the efficiency almost doubled with n-PbI_2 method, rising from 5.9% to 10.1%. Furthermore, Fig. 6b gives the histogram plots of PCE (solar cells based on n-PbI_2), showing the average PCE is ~8%. More information about V_{oc} and J_{sc} statistics are shown in Fig. S8,† demonstrating their average at 17 mA cm^{-2} and 0.85 V, respectively. IPCE spectra of perovskite solar cells with medium performance are shown in Fig. S9,† and the measured J_{sc} from the *J–V* curves agree well with the integrated J_{sc} from IPCE spectra. Further improvement of device performance may lie in the optimization of hole transport layers, such as replacing P3HT with Spiro-MeoTAD.[48] The nanoporous PbI_2 assisted two-step method accelerates the conversion of PbI_2 into perovskite significantly compared to conventional method, and the resultant perovskite films are comparatively compact. Therefore, this method can be applied to prepare phase-pure compact planar perovskite films in short time, overcoming the disadvantages of the conventional two-step method. Moreover, this method is promising to fabricate perovskite films with interpenetrating nanopores by controlling the porosity and pore size of PbI_2. And that will lead to realizing a new kind of perovskite solar cells with porous perovskite p–n heterojunction, in which porous perovskite layer is infiltrated with transparent charge transport material.[49]

Conclusion

We have demonstrated a facile way to prepare nanoporous PbI_2 films with the SSE method, which effectively accelerates the reaction between PbI_2 and MAI. Insights into the mechanism of preparing nanoporous PbI_2 films with the SSE method are provided, suggesting that the nanoporous morphology of PbI_2 comes from the synergic effect of volume shrink effect and fast crystallization from outside to inside. Using this method, we are able to prepare well-crystallized nanoporous PbI_2 films within seconds without annealing. Furthermore, we applied the nanoporous PbI_2 to preparing perovskite films, showing that most part of PbI_2 has converted into perovskite within 10 s. Based on this, an interface-limited reaction model is proposed in the reaction system of PbI_2(s)–MAI(l). Moreover, a pinhole-free perovskite overlayer is obtained, due to the volume expansion effect in the conversion of PbI_2 into perovskite. As a result, a champion PCE over 10% has been achieved. This study uncovers the PbI_2-morphology-related kinetics in the two-step deposition method, and may open up a promising avenue for preparing high quality perovskite films by controlling the properties of PbI_2 films.

Acknowledgements

This work was supported by the National Basic Research Program of China (2012CB932303), the National Natural Science Foundation of China (Grant No. 51272265, 61574148) and the Leading Youth Talent Project of Jiading District (2013).

Notes and references

1 S. de Wolf, J. Holovsky, S. Moon, P. Löper, B. Niesen, M. Ledinsky, F. Haug, J. Yum and C. Ballif, *J. Phys. Chem. Lett.*, 2014, **5**, 1035–1039.
2 S. D. Stranks, G. E. Eperon, G. Grancini, C. Menelaou, M. J. P. Alcocer, T. Leijtens, L. M. Herz, A. Petrozza and H. J. Snaith, *Science*, 2013, **342**, 341–344.
3 G. Xing, N. Mathews, S. Sun, S. S. Lim, Y. M. Lam, M. Gratzel, S. Mhaisalkar and T. C. Sum, *Science*, 2013, **342**, 344–347.
4 D. Shi, V. Adinolfi, R. Comin, M. Yuan, E. Alarousu, A. Buin, Y. Chen, S. Hoogland, A. Rothenberger, K. Katsiev, Y. Losovyj, X. Zhang, P. A. Dowben, O. F. Mohammed, E. H. Sargent and O. M. Bakr, *Science*, 2015, **347**, 519–522.

5 G. E. Eperon, S. D. Stranks, C. Menelaou, M. B. Johnston, L. M. Herz and H. J. Snaith, *Energy Environ. Sci.*, 2014, **7**, 982–988.
6 Y. Ogomi, A. Morita, S. Tsukamoto, T. Saitho, N. Fujikawa, Q. Shen, T. Toyoda, K. Yoshino, S. S. Pandey, T. Ma and S. Hayase, *J. Phys. Chem. Lett.*, 2014, **5**, 1004–1011.
7 N. Pellet, P. Gao, G. Gregori, T. Yang, M. K. Nazeeruddin, J. Maier and M. Grätzel, *Angew. Chem., Int. Ed.*, 2014, **53**, 3151–3157.
8 J. H. Noh, S. H. Im, J. H. Heo, T. N. Mandal and S. I. Seok, *Nano Lett.*, 2013, **13**, 1764–1769.
9 S. A. Kulkarni, T. Baikie, P. P. Boix, N. Yantara, N. Mathews and S. Mhaisalkar, *J. Mater. Chem. A*, 2014, **2**, 9221–9225.
10 W. S. Yang, J. H. Noh, N. J. Jeon, Y. C. Kim, S. Ryu, J. Seo and S. I. Seok, *Science*, 2015, **348**, 1234–1237.
11 H. Kim, C. Lee, J. Im, K. Lee, T. Moehl, A. Marchioro, S. Moon, R. Humphry-Baker, J. Yum, J. E. Moser, M. Graetzel and N. Park, *Sci. Rep.*, 2012, **2**, 591.
12 M. M. Lee, J. Teuscher, T. Miyasaka, T. N. Murakami and H. J. Snaith, *Science*, 2012, **338**, 643–647.
13 J. Burschka, N. Pellet, S. Moon, R. Humphry-Baker, P. Gao, M. K. Nazeeruddin and M. Grätzel, *Nature*, 2013, **499**, 316–319.
14 M. Liu, M. B. Johnston and H. J. Snaith, *Nature*, 2013, **501**, 395–398.
15 Q. Chen, H. Zhou, Z. Hong, S. Luo, H. Duan, H. Wang, Y. Liu, G. Li and Y. Yang, *J. Am. Chem. Soc.*, 2014, **136**, 622–625.
16 J. Im, H. Kim and N. Park, *APL Mater.*, 2014, **2**, 081510.
17 N. Yantara, D. Sabba, F. Yanan, J. M. Kadro, T. Moehl, P. P. Boix, S. Mhaisalkar, M. Gratzel and C. Gratzel, *Chem. Commun.*, 2015, **51**, 4603–4606.
18 Y. Wu, A. Islam, X. Yang, C. Qin, J. Liu, K. Zhang, W. Peng and L. Han, *Energy Environ. Sci.*, 2014, **7**, 2934–2938.
19 N. J. Jeon, J. H. Noh, Y. C. Kim, W. S. Yang, S. Ryu and S. Il Seol, *Nat. Mater.*, 2014, **13**, 897–903.
20 G. Li, K. L. Ching, J. Y. L. Ho, M. Wong and H. Kwok, *Adv. Energy Mater.*, 2015, **5**, 1401775.
21 J. Shi, Y. Luo, H. Wei, J. Luo, J. Dong, S. Lv, J. Xiao, Y. Xu, L. Zhu, X. Xu, H. Wu, D. Li and Q. Meng, *ACS Appl. Mater. Interfaces*, 2014, **6**, 9711–9718.
22 Y. Xie, F. Shao, Y. Wang, T. Xu, D. Wang and F. Huang, *ACS Appl. Mater. Interfaces*, 2015, **7**, 12937–12942.
23 D. H. Cao, C. C. Stoumpos, C. D. Malliakas, M. J. Katz, O. K. Farha, J. T. Hupp and M. G. Kanatzidis, *APL Mater.*, 2014, **2**, 091101.
24 B. E. Cohen, S. Gamliel and L. Etgara, *APL Mater.*, 2014, **2**, 081502.
25 Y. Zhao and K. Zhu, *J. Mater. Chem. A*, 2015, **3**, 9086–9091.
26 L. Zheng, Y. Ma, S. Chu, S. Wang, B. Qu, L. Xiao, Z. Chen, Q. Gong, Z. Wu and X. Hou, *Nanoscale*, 2014, **6**, 8171–8176.
27 P. Docampo, F. C. Hanusch, S. D. Stranks, M. Doeblinger, J. M. Feckl, M. Ehrensperger, N. K. Minar, M. B. Johnston, H. J. Snaith and T. Bein, *Adv. Energy Mater.*, 2014, **4**, 1400355.
28 J. Xi, Z. Wu, H. Dong, B. Xia, F. Yuan, B. Jiao, L. Xiao, Q. Gong and X. Hou, *Nanoscale*, 2015, **7**, 10699–10707.
29 F. Fu, L. Kranz, S. Yoon, J. Löckinger, T. Jäger, J. Perrenoud, T. Feurer, C. Gretener, S. Bücheler and A. N. Tiwari, *Phys. Status Solidi A*, 2015, **8**, 816–821.
30 C. Ying, C. Shi, N. Wu, J. Zhang and M. Wang, *Nanoscale*, 2015, **7**, 12092–12095.
31 Y. Zhou, M. Yang, A. L. Vasiliev, H. F. Garces, Y. Zhao, D. Wang, S. Pang, K. Zhu and N. P. Padture, *J. Mater. Chem. A*, 2015, **3**, 9249–9256.
32 Y. Zhou, M. Yang, W. Wu, A. L. Vasiliev, K. Zhu and N. P. Padture, *J. Mater. Chem. A*, 2015, **3**, 8178–8184.
33 P. Docampo, J. M. Ball, M. Darwich, G. E. Eperon and H. J. Snaith, *Nat. Commun.*, 2013, **4**, 2761.
34 J. H. Heo and S. H. Im, *Phys. Status Solidi RRL*, 2014, **8**, 816–821.
35 T. Du, N. Wang, H. Chen, H. Lin and H. He, *ACS Appl. Mater. Interfaces*, 2015, **7**, 3382–3388.
36 Z. Xiao, C. Bi, Y. Shao, Q. Dong, Q. Wang, Y. Yuan, C. Wang, Y. Gao and J. Huang, *Energy Environ. Sci.*, 2014, **7**, 2619–2623.
37 A. Wakamiya, M. Endo, T. Sasamori, N. Tokitoh, Y. Ogomi, S. Hayase and Y. Murata, *Chem. Lett.*, 2014, **43**, 711–713.
38 D. Shen, X. Yu, X. Cai, M. Peng, Y. Ma, X. Su, L. Xiao and D. Zou, *J. Mater. Chem. A*, 2014, **2**, 20454–20461.
39 T. Baikie, Y. Fang, J. M. Kadro, M. Schreyer, F. Wei, S. G. Mhaisalkar, M. Graetzel and T. J. White, *J. Mater. Chem. A*, 2013, **1**, 5628–5641.
40 Q. Chen, H. Zhou, T. Song, S. Luo, Z. Hong, H. Duan, L. Dou, Y. Liu and Y. Yang, *Nano Lett.*, 2014, **14**, 4158–4163.
41 N. Marinova, W. Tress, R. Humphry-Baker, M. I. Dar, V. Bojinov, S. M. Zakeeruddin, M. K. Nazeeruddin and M. Grätzel, *ACS Nano*, 2015, **9**, 4200–4209.
42 J. Schlipf, P. Docampo, C. J. Schaffer, V. Körstgens, L. Bießmann, F. Hanusch, N. Giesbrecht, S. Bernstorff, T. Bein and P. Müller-Buschbaum, *J. Phys. Chem. Lett.*, 2015, 1265–1269.
43 Y. Zhao and K. Zhu, *J. Phys. Chem. Lett.*, 2014, **5**, 4175–4186.
44 H. Ko, J. Lee and N. Park, *J. Mater. Chem. A*, 2015, **3**, 8808–8815.
45 D. Liu, M. K. Gangishetty and T. L. Kelly, *J. Mater. Chem. A*, 2014, **2**, 19873–19881.
46 Y. Han, S. Meyer, Y. Dkhissi, K. Weber, J. M. Pringle, U. Bach, L. Spiccia and Y. Cheng, *J. Mater. Chem. A*, 2015, **3**, 8139–8147.
47 B. Chen, Y. Deng, H. Tong and J. Ma, *Superlattices Microstruct.*, 2014, **69**, 194–203.
48 D. Bi, L. Yang, G. Boschloo, A. Hagfeldt and E. M. J. Johansson, *J. Phys. Chem. Lett.*, 2013, **4**, 1532–1536.
49 H. J. Snaith, *J. Phys. Chem. Lett.*, 2013, **4**, 3623–3630.